Available online at www.sciencedirect.com
SCIENCE DIRECT®
ELSEVIER
International Journal of Solids and Structures 43 (2006) 4154–4174
INTERNATIONAL JOURNAL OF SOLIDS and STRUCTURES
www.elsevier.com/locate/ijsolstr

Improved theoretical solution for interfacial stresses in concrete beams strengthened with FRP plate

Tounsi Abdelouahed *

Laboratoire des Matériaux et Hydrologie, Université de Sidi Bel Abbes, BP 89 Cité Ben M'hidi, 22000 Sidi Bel Abbes, Algeria

Received 31 March 2005
Available online 23 May 2005

Abstract

In this paper, an improved theoretical interfacial stress analysis is presented for simply supported concrete beam bonded with a FRP plate. The adherend shear deformations have been included in the present theoretical analyses by assuming a linear shear stress through the thickness of the adherends, while all existing solutions neglect this effect. Remarkable effect of shear deformations of adherends has been noted in the results. Indeed, the resulting interfacial stresses concentrations are considerably smaller than those obtained by other models which neglect adherent shear deformations. It is shown that both the normal and shear stresses at the interface are influenced by the material and geometry parameters of the composite beam. This research is helpful for the understanding on mechanical behavior of the interface and design of the FRP–RC hybrid structures.

Keywords: FRP composites; Interfacial stresses; Plate bonding; Concrete beam; Strengthening; Improved model

1. Introduction

Fiber reinforced plastics (FRP) materials have been recognized as new innovative materials for concrete rehabilitation and retrofit. Since concrete is poor in tension, a beam without any form of reinforcement will fail when subjected to a relatively small tensile load. Therefore, the use of the FRP to strengthen the concrete is an effective solution to increase the overall strength of the structure. In recent years, many studies have been carried out on this retrofitting method (e.g. An et al., 1991; Saadatmanesh and Ehsani, 1991; Sharif et al., 1994; Chajes et al., 1994; Quantrill et al., 1996a,b; Arduini and Nanni, 1997; Wu et al.,

* Tel.: +213 48 56 54 44; fax: +213 48 54 43 44.
E-mail address: tou_abdel@yahoo.com

0020-7683/$ - see front matter © 2005 Elsevier Ltd. All rights reserved.
doi:10.1016/j.ijsolstr.2005.03.074

Nomenclature

A_i $(i = 1,2)$ the cross-sectional area of adherend "i"
E_i $(i = 1,2)$ the elastic modulus of adherend "i"
E_a the elastic modulus of adhesive
G_a the transverse shear moduli of adhesive
G_i $(i = 1,2)$ the transverse shear moduli of the adherend "i"
I the second moment of area
K_S the shear stiffness of the adhesive
K_n normal stiffness of the adhesive per unit length
$M(x)$ the bending moment
$M_T(x)$ the total applied moment
N_i $(i = 1,2)$ the longitudinal resultant force for adherend "i"
P the concentrated load
$U_i^N(x,y)$ $(i = 1,2)$ longitudinal displacements in adherend "i" induced by the longitudinal forces
$V(x)$ shear force
W_i^N $(i = 1,2)$ the transverse displacement in adherend "i" induced by the longitudinal forces
b_2 the width of the soffit plate
q the uniformly distributed load
t_i $(i = 1,2)$ the thickness of adherend "i"
t_a the thickness of adhesive
u_1 the longitudinal displacement at the base of adherend 1
u_2 the longitudinal displacement at the top of adherend 2
u_1^N the longitudinal displacement induced by the longitudinal forces at the interface between the upper adherend and the adhesive
u_2^N the longitudinal displacement induced by the longitudinal forces at the interface between the lower adherend and the adhesive
w_i $(i = 1,2)$ vertical displacements of adherend "i"
y_i $(i = 1,2)$ distances from the bottom of adherend 1 and the top of adherend 2 to their respective centroid
ε_1 strain at the base of adherend 1
ε_2 strain at the top of adherend 2
ε_i^M $(i = 1,2)$ strains induced by the bending moment at the adherend "i"
ε_i^N $(i = 1,2)$ strains induced by the longitudinal forces at the adherend "i"
$\sigma_{xy(i)}$ $(i = 1,2)$ the shear stresses in adherend "i"
σ_n the normal stress in the adhesive
γ_i $(i = 1,2)$ the shear strain in adherend "i"
τ_a the shear stresses through the thickness of adhesive
σ_i^N $(i = 1,2)$ longitudinal normal stresses for adherend "i"

1997, 2002; Malek et al., 1998; Saadatmanesh and Malek, 1998; Spadea et al., 1998; Triantafillou and Antonopoulos, 2000; Chen and Teng, 2001, 2003; Bakis et al., 2002; Smith and Teng, 2002a,b). This plate bonding technique has many advantages including ease of application due to the high strength-to-weight ratio of FRPs, minimization of disturbances to existing operations, and high corrosion resistance. An important failure mode for such strengthened members is the debonding of the FRP plate from the member because of high interfacial stresses near the plate end. Important contributions on debonding strength models have

been made by Oehlers (1992), Baluch et al. (1995) and Raoof et al. (2000) for RC beams bonded with steel plates and Smith and Teng (2002a,b), Saadatmanesh and Malek (1998), Yuan et al. (2004) and Gao et al. (2005) for RC beams bonded with FRP plates. Accurate predictions of interfacial stresses are thus important for designing against debonding failures. Ascione and Feo (2000) developed a finite element model to predict the shear and the normal stresses in the adhesive layer of plated reinforced concrete beams and the numerical results agreed with the experimental results obtained by Jones et al. (1988) and the theoretical results presented by Roberts (1989). Roberts and Haji-Kazemi (1989) proposed an analytical solution based on partial interaction theory, for predicting the shear and normal stress concentrations in adhesive joints. This solution is for a uniformly distributed load only. Taljsten (1997) proposed a solution based on direct deformation compatibility to determine the interfacial stresses. Smith and Teng (2001), having carried out a review of the approximate closed-form solutions for interfacial stresses in literature, presented a new solution which was intended for application to beams with a bonded thin plate. The new solution of Smith and Teng (2001) seems that it is the more accurate widely applicable solution, particularly when the flexural stiffness of the bonded plate becomes significant. Shen et al. (2001) have developed a complementary energy method to study the interfacial stresses for simply supported RC beams and slabs bonded with a thin composite plate or steel plate. Rabinovich and Frostig (2000) and Yang et al. (2002) presented closed-form high-order analyses of reinforced concrete beams strengthened with FRP plates, which satisfy the free surface condition at the ends of the adhesive layer. The solution methodology is general in nature and can be applied to the analysis of other types of composite structure.

The objective of this investigation is to improve the famous method developed by Smith and Teng (2001) by incorporating with the adherend shear deformations. Indeed, it is reasonable to assume that the shear stresses, which develop in the adhesive, are continuous across the adhesive–adherend interface. In addition, equilibrium requires the shear stress be zero at the free surface. The importance of including shear-lag effect of the adherents was shown by Tsai et al. (1998). These latter, have used the same theory presented here, to study adhesive lap joints. The obtained results are in good agreement with those of experimental and numerical results. Shear deformation in the adherents are ignored in the models mentioned above, possibly due to the relatively small values compared to longitudinal normal deformations in some cases, or due to the complexity of formulation. The experimental results presented by Jones et al. (1988) and those of Ascione and Feo (2000) using finite element method show that the shear stress reduce to zero in cut-off section. However, the methods developed by Malek et al. (1998), Roberts (1989), Roberts and Haji-Kazemi (1989), Taljsten (1997) and Smith and Teng (2001) predict maximum values for the shear stresses at the same section. The presented method predicts also, maximum values in cut-off section, but comparatively to those of the cited methods above, the computed interfacial stresses are considerably smaller than those obtained by other models which neglect adherent shear deformations. Hence, the adopted improved model describes better actual response of the FRP–RC hybrid beams and permits the evaluation of the interfacial stresses, the knowledge of which is very important in the design of such structures.

2. Research significance

The most common failure modes for FRP-strengthened RC beams are debonding of the FRP plate or ripping of the concrete cover. These types of failures prevent the strengthened beam for reaching its ultimate flexural capacity, and therefore they must be included in design considerations. Both of these premature failure modes are caused by shear and normal stress concentrations in adhesive layer. Closed form solutions of stress concentrations are required in developing design guidelines for strengthening reinforced concrete beams with FRP plates.

3. Theoretical derivation

A differential section dx, can be cut out from the FRP strengthened concrete beam (Fig. 1) as shown in Fig. 2. The composite beam is made from three materials: concrete (or RC concrete), adhesive layer and FRP reinforcement. In the present analysis, linear elastic behaviour is regarded to be for all the materials; the adhesive is assumed to only play a role in transferring the stresses from the concrete to the FRP reinforcement and the stresses in the adhesive layer do not change through the direction of the thickness.

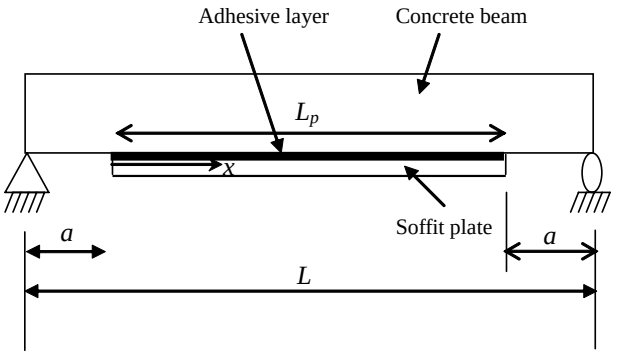

Fig. 1. Simply supported beam strengthened with bonded plate.

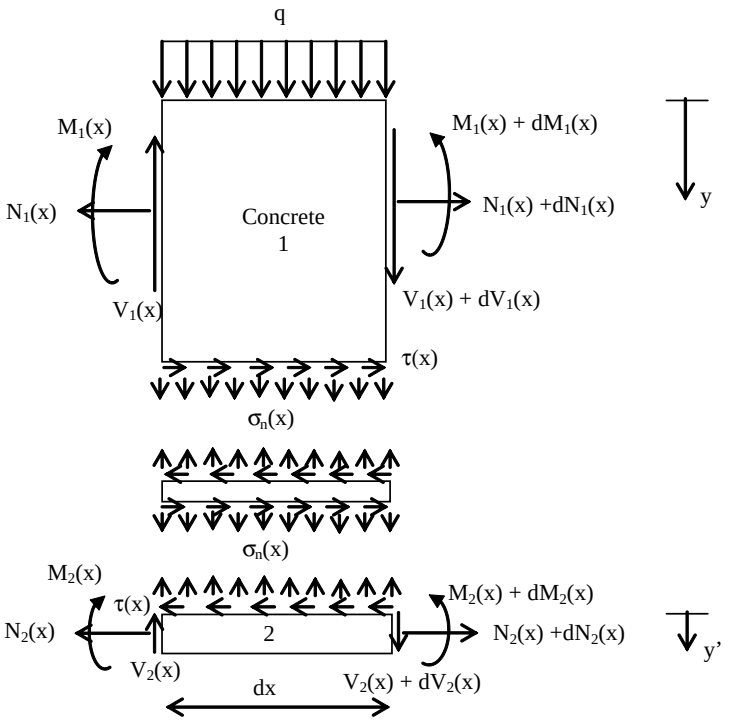

Fig. 2. Forces in infinitesimal element of a soffit-plated beam.

3.1. Shear stress distribution along the FRP–concrete interface

The strains in the concrete near the adhesive interface and the external FRP reinforcement can be expressed as, respectively:

$$\varepsilon_1(x) = \frac{\mathrm{d}u_1(x)}{\mathrm{d}x} = \varepsilon_1^M(x) + \varepsilon_1^N(x) \tag{1}$$

$$\varepsilon_2(x) = \frac{\mathrm{d}u_2(x)}{\mathrm{d}x} = \varepsilon_2^M(x) + \varepsilon_2^N(x) \tag{2}$$

where $u_1(x)$ and $u_2(x)$ are the longitudinal displacements at the base of adherend 1 and the top of adherend 2, respectively. $\varepsilon_1^M(x)$ and $\varepsilon_2^M(x)$ are the strains induced by the bending moment at the adherend 1 and 2, respectively and they are written as follow:

$$\varepsilon_1^M(x) = \frac{y_1}{E_1 I_1} M_1(x) \quad \text{and} \quad \varepsilon_2^M(x) = \frac{-y_2}{E_2 I_2} M_2(x) \tag{3}$$

where E is the elastic modulus and I the second moment of area. The subscripts 1 and 2 denote adherends 1 and 2, respectively. $M(x)$ is the bending moment while y_1 and y_2 are the distances from the bottom of adherend 1 and the top of adherend 2 to their respective centroid.

$\varepsilon_1^N(x)$ and $\varepsilon_2^N(x)$ are the unknowns longitudinal strains of the concrete and FRP reinforcement, respectively, at the adhesive interface and they are due to the longitudinal forces. These strains are given as follow:

$$\varepsilon_1^N(x) = \frac{\mathrm{d}u_1^N(x)}{\mathrm{d}x}; \quad \varepsilon_2^N(x) = \frac{\mathrm{d}u_2^N(x)}{\mathrm{d}x} \tag{4}$$

where $u_1^N(u_2^N)$ represents the longitudinal force-induced adhesive displacement at the interface between the upper (lower) adherend and the adhesive.

To determine the unknowns longitudinal strains $\varepsilon_1^N(x)$ and $\varepsilon_2^N(x)$, shear deformations of the adherends are incorporated in this analysis. It is reasonable to assume that the shear stresses, which develop in the adhesive, are continuous across the adhesive–adherend interface. In addition, equilibrium requires the shear stress be zero at the free surface. Using the same methodology developed by Tsai et al. (1998), this effect is taken into account. A parabolic variation of longitudinal displacements $U_1^N(x,y)$ and $U_2^N(x,y)$ in both adherends (concrete beam and soffit plate) is assumed.

$$U_1^N(x,y) = A_1(x)y^2 + B_1(x)y + C_1(x) \tag{5}$$

$$U_2^N(x,y') = A_2(x)y'^2 + B_2(x)y' + C_2(x) \tag{6}$$

where $y(y')$ is a local coordinate system with the origin at the top surface of the upper (lower) adherend Fig. 2.

The shear stresses in the two adherends are given by

$$\sigma_{xy(1)} = G_1\gamma_{xy(1)} \tag{7}$$

$$\sigma_{xy'(2)} = G_2\gamma_{xy'(2)} \tag{8}$$

With

$$\gamma_{xy(i)} = \frac{\partial U_i^N}{\partial y} + \frac{\partial W_i^N}{\partial x}; \quad i = 1,2 \tag{9}$$

G_1 and G_2 are the transverse shear moduli of the adherend 1 and 2, respectively. Neglecting the variations of transverse displacement W_i^N (induced by the longitudinal forces) with the longitudinal coordinate x.

$$\gamma_{xy(i)} \approx \frac{\partial U_i^N}{\partial y} \tag{10}$$

and the shear stresses are expressed as

$$\sigma_{xy(1)} = G_1(2A_1y + B_1) \tag{11}$$

$$\sigma_{xy'(2)} = G_2(2A_2y' + B_2) \tag{12}$$

The shear stresses must satisfy the following conditions:

$$\sigma_{xy(1)}(x, t_1) = \sigma_{xy'(2)}(x, 0) = \tau(x) = \tau_a \tag{13}$$

$$\sigma_{xy(1)}(x, 0) = 0, \quad \sigma_{xy'(2)}(x, t_2) = 0 \tag{14}$$

t_1, t_2 are the thickness of adherend 1 and 2, respectively.

Condition (13) follows from continuity and the assumption of the uniform shear stresses ($\tau(x) = \tau_a$) through the thickness of adhesive. Condition (14) states there is no shear stresses at the top surface of the adherend 1 (i.e. at $y = 0$) and at the bottom surface at the adherend 2 (i.e. at $y' = t_2$). These conditions yield

$$\sigma_{xy(1)} = \frac{\tau(x)}{t_1}y \tag{15}$$

$$\sigma_{xy'(2)} = \left(1 - \frac{y'}{t_2}\right)\tau(x) \tag{16}$$

Then with a linear material constitutive relationship the adherend shear strain γ_1 for the adherend 1 and γ_2 for the adherend 2 are written as

$$\gamma_{xy(1)} = \gamma_1 = \frac{\tau_a}{G_1 t_1}y \tag{17}$$

$$\gamma_{xy'(2)} = \gamma_2 = \frac{\tau_a}{G_2}\left(1 - \frac{y'}{t_2}\right) \tag{18}$$

The longitudinal displacement functions U_1^N for the upper adherend and U_2^N for the lower adherend, due to the longitudinal forces, are given by

$$U_1^N(y) = U_1^N(0) + \int_0^y \gamma_1(y)\,dy = U_1^N(0) + \frac{\tau_a}{2G_1 t_1}y^2 \tag{19}$$

$$U_2^N(y') = u_2^N + \int_0^{y'} \gamma_2(y')\,dy' = u_2^N + \frac{\tau_a}{G_2}\left(y' - \frac{y'^2}{2t_2}\right) \tag{20}$$

where $U_1^N(0)$ represents the displacement at the top surface of the upper adherend (due to the longitudinal forces) and u_2^N is the longitudinal force-induced adhesive displacement at the interface between the adhesive and lower adherend.

Note that due to the perfect bonding of the joints, the displacements are continuous at the interfaces between the adhesive and adherends. As a result, the u_2^N should be equivalent to the lower adherend displacement at the interface and u_1^N (the adhesive displacement at the interface between the adhesive and upper adherend) should be the same as the upper adherend displacement at the interface. Based on Eq. (19) the u_1^N can be expressed as

$$u_1^N = U_1^N(y = t_1) = U_1^N(0) + \frac{\tau_a t_1}{2G_1} \tag{21}$$

Using Eq. (21), Eq. (19) can be rewritten as

$$U_1^N(y) = u_1^N + \frac{\tau_a}{2G_1 t_1}y^2 - \frac{\tau_a t_1}{2G_1} \tag{22}$$

The longitudinal resultant forces, N_1 and N_2 for the upper and lower adherends, respectively, are

$$N_1 = b_1 \int_0^{t_1} \sigma_1^N(y)\,\mathrm{d}y \tag{23}$$

and

$$N_2 = b_2 \int_0^{t_2} \sigma_2^N(y')\,\mathrm{d}y' \tag{24}$$

where σ_1^N and σ_2^N are longitudinal normal stresses for the upper and lower adherends, respectively. By changing these stresses into functions of displacements and substituting Eqs. (20) and (22) into the displacements, Eqs. (23) and (24) can be rewritten as

$$N_1 = E_1 b_1 \int_0^{t_1} \frac{\mathrm{d}U_1^N}{\mathrm{d}x}\,\mathrm{d}y = E_1 A_1 \left(\frac{\mathrm{d}u_1^N}{\mathrm{d}x} - \frac{t_1}{3G_1}\frac{\mathrm{d}\tau_a}{\mathrm{d}x}\right) \tag{25}$$

and

$$N_2 = E_2 b_2 \int_0^{t_2} \frac{\mathrm{d}U_2^N}{\mathrm{d}x}\,\mathrm{d}y' = E_2 A_2 \left(\frac{\mathrm{d}u_2^N}{\mathrm{d}x} + \frac{t_2}{3G_2}\frac{\mathrm{d}\tau_a}{\mathrm{d}x}\right) \tag{26}$$

Hence, the longitudinal strains induced by the longitudinal forces Eq. (4) can be expressed as

$$\varepsilon_1^N(x) = \frac{\mathrm{d}u_1^N(x)}{\mathrm{d}x} = \frac{N_1}{E_1 A_1} + \frac{t_1}{3G_1}\frac{\mathrm{d}\tau_a}{\mathrm{d}x} \tag{27}$$

$$\varepsilon_2^N(x) = \frac{\mathrm{d}u_2^N(x)}{\mathrm{d}x} = \frac{N_2}{E_2 A_2} - \frac{t_2}{3G_2}\frac{\mathrm{d}\tau_a}{\mathrm{d}x} \tag{28}$$

Substituting Eqs. (27), (28) and (3) into Eqs. (1) and (2), respectively, these latter become:

$$\varepsilon_1(x) = \frac{\mathrm{d}u_1(x)}{\mathrm{d}x} = \frac{y_1}{E_1 I_1} M_1(x) + \frac{N_1(x)}{E_1 A_1} + \frac{t_1}{3G_1}\frac{\mathrm{d}\tau(x)}{\mathrm{d}x} \tag{29}$$

$$\varepsilon_2(x) = \frac{\mathrm{d}u_2(x)}{\mathrm{d}x} = \frac{-y_2}{E_2 I_2} M_2(x) + \frac{N_2(x)}{E_2 A_2} - \frac{t_2}{3G_2}\frac{\mathrm{d}\tau(x)}{\mathrm{d}x} \tag{30}$$

where $N(x)$ are the axial forces in each adherend, A the cross-sectional area.

The shear stress in the adhesive can be expressed as follows:

$$\tau_a = \tau(x) = K_S[u_2(x) - u_1(x)] \tag{31}$$

where $K_S = \frac{G_a}{t_a}$ is shear stiffness of the adhesive, G_a and t_a are shear modulus and thickness of the adhesive, respectively; $u_1(x)$ and $u_2(x)$ are the longitudinal displacements at the base of adherend 1 and the top of adherend 2. Differentiating the above expression we obtain

$$\frac{\mathrm{d}\tau(x)}{\mathrm{d}x} = K_S\left[\frac{\mathrm{d}u_2(x)}{\mathrm{d}x} - \frac{\mathrm{d}u_1(x)}{\mathrm{d}x}\right] \tag{32}$$

Consideration of horizontal equilibrium gives:

$$\frac{\mathrm{d}N_1(x)}{\mathrm{d}x} = -b_2\tau(x) \tag{33}$$

$$\frac{\mathrm{d}N_2(x)}{\mathrm{d}x} = b_2\tau(x) \tag{34}$$

where

$$N_2(x) = N(x) = b_2 \int_0^x \tau(x) \tag{35}$$

and

$$N_1(x) = -N(x) = -b_2 \int_0^x \tau(x) \tag{36}$$

b_2 is the width of the soffit plate.

Assuming equal curvature in the beam and soffit plate, the relationship between the moments in the two adherends can be expressed as

$$M_1(x) = RM_2(x) \tag{37}$$

With

$$R = \frac{E_1 I_1}{E_2 I_2} \tag{38}$$

Moment equilibrium of the differential segment of the plated beam in Fig. 2 gives:

$$M_T(x) = M_1(x) + M_2(x) + N(x)(y_1 + y_2 + t_a) \tag{39}$$

where $M_T(x)$ is the total applied moment.

The bending moment in each adherend, expressed as a function of the total applied moment and the interfacial shear stress, is given as

$$M_1(x) = \frac{R}{R+1}\left[M_T(x) - b_2 \int_0^x \tau(x)(y_1 + y_2 + t_a)\,dx\right] \tag{40}$$

and

$$M_2(x) = \frac{1}{R+1}\left[M_T(x) - b_2 \int_0^x \tau(x)(y_1 + y_2 + t_a)\,dx\right] \tag{41}$$

The first derivative of the bending moment in each adherend gives:

$$\frac{dM_1(x)}{dx} = \frac{R}{R+1}[V_T(x) - b_2\tau(x)(y_1 + y_2 + t_a)] \tag{42}$$

and

$$\frac{dM_2(x)}{dx} = \frac{1}{R+1}[V_T(x) - b_2\tau(x)(y_1 + y_2 + t_a)] \tag{43}$$

Substituting Eqs. (29) and (30) into Eq. (32) and differentiating the resulting equation once yields:

$$\frac{d^2\tau(x)}{dx^2} = K_S\left(\frac{-y_2}{E_2 I_2}\frac{dM_2(x)}{dx} + \frac{1}{E_2 A_2}\frac{dN_2(x)}{dx} - \frac{y_1}{E_1 I_1}\frac{dM_1(x)}{dx} - \frac{1}{E_1 A_1}\frac{dN_1(x)}{dx}\right) - K_S\left(\frac{t_2}{3G_2} + \frac{t_1}{3G_1}\right)\frac{d^2\tau(x)}{dx^2} \tag{44}$$

Substitution of the shear forces (Eqs. (42) and (43)) and axial forces (Eqs. (35) and (36)) into Eq. (44) gives the following governing differential equation for the interfacial shear stress.

$$\frac{d^2\tau(x)}{dx^2} - K_1 b_2\left(\frac{(y_1 + y_2)(y_1 + y_2 + t_a)}{E_1 I_1 + E_2 I_2} + \frac{1}{E_1 A_1} + \frac{1}{E_2 A_2}\right)\tau(x) + K_1\left(\frac{y_1 + y_2}{E_1 I_1 + E_2 I_2}\right)V_T(x) = 0 \tag{45}$$

where

$$K_1 = \frac{1}{\left(\frac{t_a}{G_a} + \frac{t_1}{3G_1} + \frac{t_2}{3G_2}\right)} \tag{46}$$

For simplicity, the general solutions presented below are limited to loading which is either concentrated or uniformly distributed over part or the whole span of the beam, or both. For such loading, $d^2V_T(x)/dx^2 = 0$, and the general solution to Eq. (45) is given by

$$\tau(x) = B_1 \cosh(\lambda x) + B_2 \sinh(\lambda x) + m_1 V_T(x) \tag{47}$$

where

$$\lambda^2 = K_1 b_2 \left(\frac{(y_1 + y_2)(y_1 + y_2 + t_a)}{E_1 I_1 + E_2 I_2} + \frac{1}{E_1 A_1} + \frac{1}{E_2 A_2}\right) \tag{48}$$

and

$$m_1 = \frac{K_1}{\lambda^2}\left(\frac{y_1 + y_2}{E_1 I_1 + E_2 I_2}\right) \tag{49}$$

B_1 and B_2 are constant coefficients determined from the boundary conditions.

3.2. Normal stress distribution along the FRP–concrete interface

The normal stress in the adhesive can be expressed as follows:

$$\sigma_n(x) = K_n \Delta w(x) = K_n[w_2(x) - w_1(x)] \tag{50}$$

where K_n is normal stiffness of the adhesive per unit length and can be deduced as

$$K_n = \frac{\sigma_n(x)}{\Delta w(x)} = \frac{\sigma_n(x)}{\Delta w(x)/t_a}\left(\frac{1}{t_a}\right) = \frac{E_a}{t_a} \tag{51}$$

$w_1(x)$ and $w_2(x)$ are the vertical displacements of adherend 1 and 2, respectively.

Differentiating Eq. (50) twice results in

$$\frac{d^2\sigma_n(x)}{dx^2} = K_n\left[\frac{d^2w_2(x)}{dx^2} - \frac{d^2w_1(x)}{dx^2}\right] \tag{52}$$

Considering the moment–curvature relationships for the beam to be strengthened and the external reinforcement, respectively:

$$\frac{d^2w_1(x)}{dx^2} = -\frac{M_1(x)}{E_1 I_1}, \quad \frac{d^2w_2(x)}{dx^2} = -\frac{M_2(x)}{E_2 I_2} \tag{53}$$

The equilibrium of adherend 1 and 2, leads to the following relationships:

Adherend 1:

$$\frac{dM_1(x)}{dx} = V_1(x) - b_2 y_1 \tau(x) \quad \text{and} \quad \frac{dV_1(x)}{dx} = -b_2\sigma_n(x) - q \tag{54}$$

Adherend 2:

$$\frac{dM_2(x)}{dx} = V_2(x) - b_2 y_2 \tau(x) \quad \text{and} \quad \frac{dV_2(x)}{dx} = b_2\sigma_n(x) \tag{55}$$

Based on the above equilibrium equations, the governing differential equations for the deflection of adherends 1 and 2, expressed in terms of the interfacial shear and normal stresses, are given as follows:

Adherend 1:

$$\frac{d^4 w_1(x)}{dx^4} = \frac{1}{E_1 I_1} b_2 \sigma(x) + \frac{y_1}{E_1 I_1} b_2 \frac{d\tau(x)}{dx} + \frac{q}{E_1 I_1} \tag{56}$$

Adherend 2:

$$\frac{d^4 w_2(x)}{dx^4} = -\frac{1}{E_2 I_2} b_2 \sigma(x) + \frac{y_2}{E_2 I_2} b_2 \frac{d\tau(x)}{dx} \tag{57}$$

Substitution of Eqs. (56) and (57) into the fourth derivation of the interfacial normal stress obtainable from Eq. (50) gives the following governing differential equation for the interfacial normal stress:

$$\frac{d^4 \sigma_n(x)}{dx^4} + \frac{E_a b_2}{t_a}\left(\frac{1}{E_1 I_1} + \frac{1}{E_2 I_2}\right)\sigma_n(x) + \frac{E_a b_2}{t_a}\left(\frac{y_1}{E_1 I_1} - \frac{y_2}{E_2 I_2}\right)\frac{d\tau(x)}{dx} + \frac{q E_a}{t_a E_1 I_1} = 0 \tag{58}$$

The general solution to this fourth-order differential equation is

$$\sigma_n(x) = e^{-\beta x}[C_1 \cos(\beta x) + C_2 \sin(\beta x)] + e^{\beta x}[C_3 \cos(\beta x) + C_4 \sin(\beta x)] - n_1 \frac{d\tau(x)}{dx} - n_2 q \tag{59}$$

For large values of x it is assumed that the normal stress approaches zero, and as a result $C_3 = C_4 = 0$. The general solution therefore becomes:

$$\sigma_n(x) = e^{-\beta x}[C_1 \cos(\beta x) + C_2 \sin(\beta x)] - n_1 \frac{d\tau(x)}{dx} - n_2 q \tag{60}$$

where

$$\beta = \sqrt[4]{\frac{E_a b_2}{4 t_a}\left(\frac{1}{E_1 I_1} + \frac{1}{E_2 I_2}\right)} \tag{61}$$

$$n_1 = \left(\frac{y_1 E_2 I_2 - y_2 E_1 I_1}{E_1 I_1 + E_2 I_2}\right) \tag{62}$$

and

$$n_2 = \frac{E_2 I_2}{b_2 (E_1 I_1 + E_2 I_2)} \tag{63}$$

C_1 and C_2 are constant coefficients determined from the boundary conditions.

3.3. Application of boundary conditions

The same loads cases used by Smith and Teng (2001) are considered in the present method.

A simply supported beam is investigated which is subjected to a uniformly distributed load and an arbitrarily positioned single point load as shown in Fig. 3. This section derives the expressions of the interfacial shear and normal stresses for each load case by applying suitable boundary conditions.

3.3.1. Interfacial shear stress for a uniformly distributed load

As is described by Smith and Teng (2001) the interfacial shear stress for this load case at any point is written as

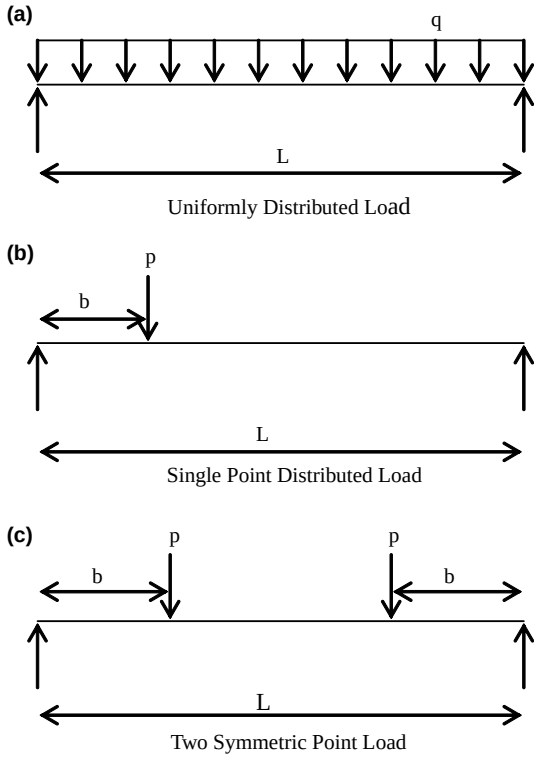

Fig. 3. Load cases.

$$\tau(x) = \left[\frac{m_2 a}{2}(L-a) - m_1\right]\frac{q e^{-\lambda x}}{\lambda} + m_1 q\left(\frac{L}{2} - a - x\right) \quad 0 \leqslant x \leqslant L_p \tag{64}$$

where q is the uniformly distributed load and x, a, L and L_p are defined in Fig. 1. Contrary, to the method presented by Smith and Teng (2001), the expression of m_2 in the present method which take into account the shear deformation of adherends become:

$$m_2 = \frac{K_1 y_1}{E_1 I_1} \tag{65}$$

3.3.2. Interfacial shear stress for a single point load

The general solution for the interfacial shear stress for this load case is (Smith and Teng, 2001):

$a < b$:

$$\tau(x) = \begin{cases} \dfrac{m_2}{\lambda} Pa\left(1 - \dfrac{b}{L}\right)e^{-\lambda x} + m_1 P\left(1 - \dfrac{b}{L}\right) - m_1 P\cosh(\lambda x)e^{-k} & 0 \leqslant x \leqslant (b-a) \\ \dfrac{m_2}{\lambda} Pa\left(1 - \dfrac{b}{L}\right)e^{-\lambda x} - m_1\dfrac{Pb}{L} + m_1 P\sinh(k)e^{-\lambda x} & (b-a) \leqslant x \leqslant L_p \end{cases} \tag{66}$$

$a > b$:

$$\tau(x) = \frac{m_2}{\lambda} Pb\left(1 - \frac{a}{L}\right)e^{-\lambda x} - m_1 P\frac{b}{L} \quad 0 \leqslant x \leqslant L_p \tag{67}$$

where P is the concentrated load and $k = \lambda(b - a)$. The expression of m_1, m_2 and, takes into consideration the shear deformation of adherends, which is neglected by Smith and Teng (2001).

3.3.3. Interfacial shear stress for two point loads

The general solution for the interfacial shear stress for this load case is (Smith and Teng, 2001):

$a < b$

$$\tau(x) = \begin{cases} \frac{m_2}{\lambda} Pa e^{-\lambda x} + m_1 P - m_1 P \cosh(\lambda x) e^{-k} & 0 \leqslant x \leqslant (b-a) \\ \frac{m_2}{\lambda} Pa e^{-\lambda x} + m_1 P \sinh(k) e^{-\lambda x} & (b-a) \leqslant x \leqslant \frac{L_p}{2} \end{cases} \tag{68}$$

$a > b$

$$\tau(x) = \frac{m_2}{\lambda} Pb e^{-\lambda x} \quad 0 \leqslant x \leqslant L_p \tag{69}$$

3.3.4. Interfacial normal stress: general expression for all three load cases

As is described by Smith and Teng (2001) the constants C_1 and C_2 in Eq. (60) are determined using the appropriate boundary conditions and they are written as follow:

$$C_1 = \frac{E_a}{2\beta^3 t_a E_1 I_1} [V_T(0) + \beta M_T(0)] - \frac{n_3}{2\beta^3}\tau(0) + \frac{n_1}{2\beta^3}\left(\frac{d^4\tau(0)}{dx^4} + \beta\frac{d^3\tau(0)}{dx^3}\right) \tag{70}$$

$$C_2 = -\frac{E_a}{2\beta^2 t_a E_1 I_1} M_T(0) - \frac{n_1}{2\beta^2}\frac{d^3\tau(0)}{dx^3} \tag{71}$$

where

$$n_3 = \frac{E_a b_2}{t_a}\left(\frac{y_1}{E_1 I_1} - \frac{y_2}{E_2 I_2}\right) \tag{72}$$

The above expressions for the constants C_1 and C_2 have been left in terms of the bending moment $M_T(0)$ and shear force $V_T(0)$ at the end of the soffit plate. With the constants C_1 and C_2 determined, the interfacial normal stress can then be found using Eq. (60) for all three load cases.

4. Comparison of predictions with experimental data

The predicted stresses by the present theory have been compared to those of experimental results obtained by Jones et al. (1988). The geometry and materials properties of the specimen are summarized in Table 1. As it can be seen from Fig. 4 the predicted theoretical results agree with the experimental results

Table 1
Dimensions and material properties

Concrete	$b_1 = 155$ mm	$t_1 = 225$ mm	$E_1 = 31{,}000$ MPa
Steel	$b_2 = 125$ mm	$t_2 = 6$ mm	$E_2 = 200{,}000$ MPa
Adhesive	$b_a = 125$ mm	$t_a = 1.5$ mm	$E_a = 280$ MPa
			$G_a = 108$ MPa

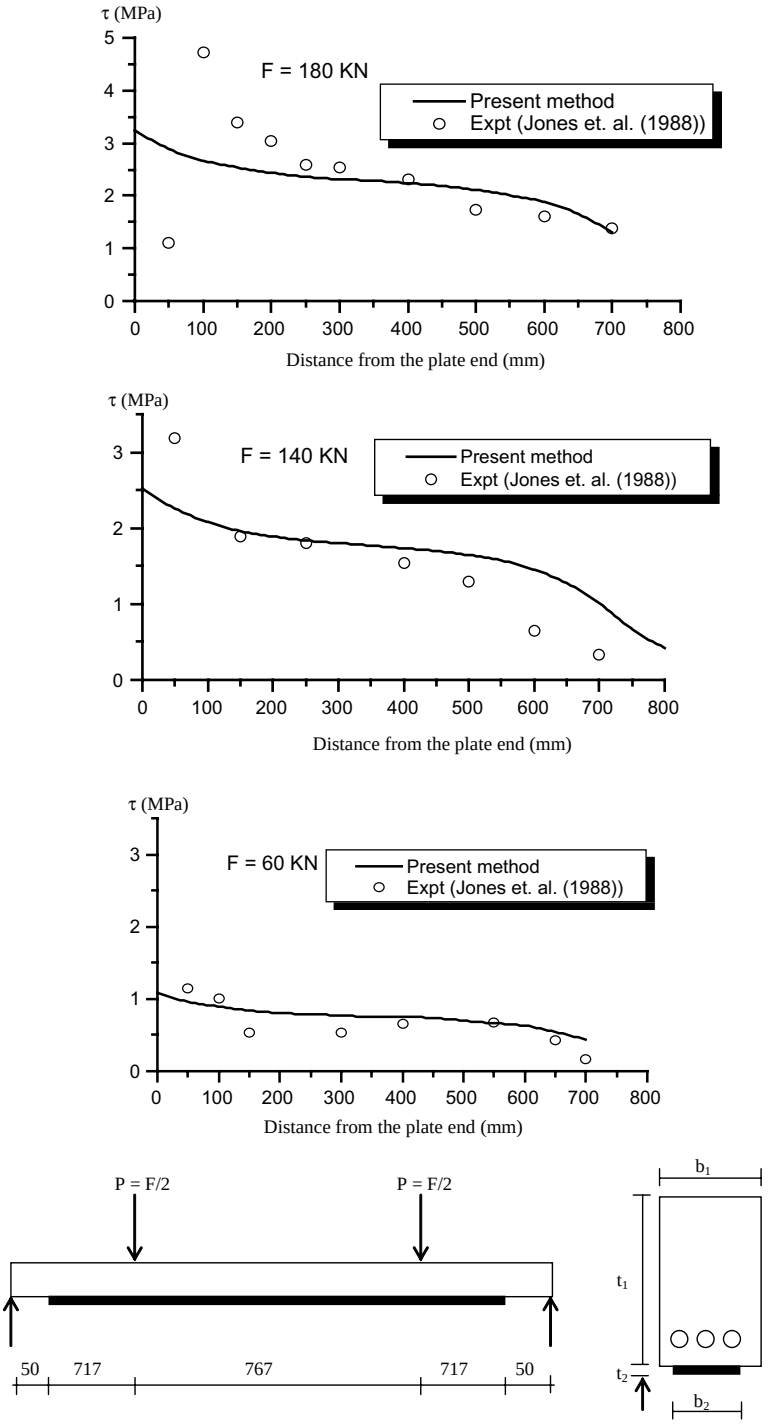

Fig. 4. Comparison of theoretical results with experimental results for beam F31 tested by Jones et al. (1988).

presented by Jones et al. (1988). The experimental results presented by Jones et al. (1988) and those of Ascione and Feo (2000) using finite element method show that the shear stress reduce to zero in cut-off section. However, the methods developed by Smith and Teng (2001), Roberts (1989) and Malek et al. (1998) predict maximum values for the shear stresses at the same section. The presented method predicts also, maximum values in cut-off section, but comparatively to those of the cited methods above, the computed interfacial stresses are considerably smaller than those obtained by other models which neglect adherent shear deformations. On the other hand, Tsai et al. (1998) have used the same theory to study adhesive lap joints. The obtained results are in good agreement with those of experimental and numerical results.

Table 2
Geometric and material properties

Component	Width (mm)	Depth (mm)	Young's modulus (MPa)	Poisson's ratio	Shear modulus (MPa)
RC beam	$b_1 = 200$	$t_1 = 300$	$E_1 = 30000$	0.18	–
Adhesive layer	$b_a = 200$	$t_a = 2.0$	$E_a = 3000$	0.35	–
GFRP plate	$b_2 = 200$	$t_2 = 4.0$	$E_2 = 50000$	0.28	$G_{12} = 5000$
CFRP plate	$b_2 = 200$	$t_2 = 4.0$	$E_2 = 140{,}000$	0.28	$G_{12} = 5000$
Steel plate	$b_2 = 200$	$t_2 = 4.0$	$E_2 = 200{,}000$	0.3	–

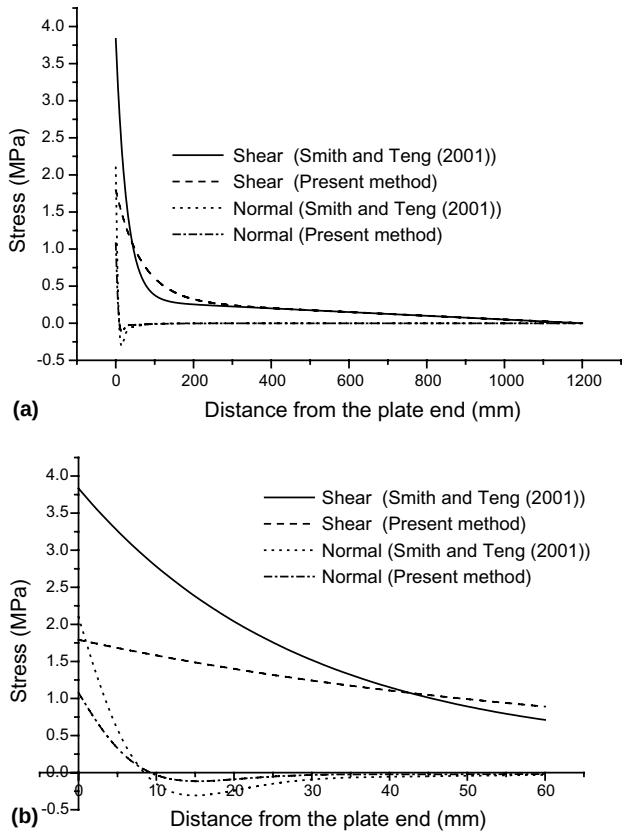

Fig. 5. Comparison of interfacial shear and normal stresses for an RC beam with a bonded CFRP soffit plate subjected to a UDL.

5. Numerical comparisons

The effect of adherend transverse shear stiffness on the maximum shear and normal stress is examined by comparing the results obtained with the present theory and those determined from the famous method developed by Smith and Teng (2001). For this, an RC beam strengthened with a glass–fiber reinforced plastic (GFRP), CFRP or steel soffit plate is analyzed. The beams are simply supported and subjected to a central point load or a uniformly distributed load. A summary of the geometric and material properties is given in Table 2. The span of RC beam is $L = 3000$ mm, the distance from the support to the end of the plate is $a = 300$ mm, the mid-point load is 150 kN and UDL is 50 kN/m.

Fig. 5 plots the interfacial shear and normal stresses for the example RC beam bonded with a CFRP plate for the UDL case, while Fig. 6 is a similar plot for the mid-point load case. Overall, the interfacial stresses predicted by the present method almost agree with those of Smith and Teng (2001), except near the free edge, where the present theory predicts lower values (Figs. 5b and 6b). Hence, it is apparent that the adherend shear deformation reduces the interfacial stresses concentration and thus renders the adhesive shear distribution more uniform. The interfacial normal stress is seen to change sign at a short distance away from the plate end.

The results of the peak interfacial shear and normal stresses (at the end of the soffit plate) are given in Tables 3 and 4 for the RC beam strengthened by bonding GFRP, CFRP or steel plate. As it can be seen

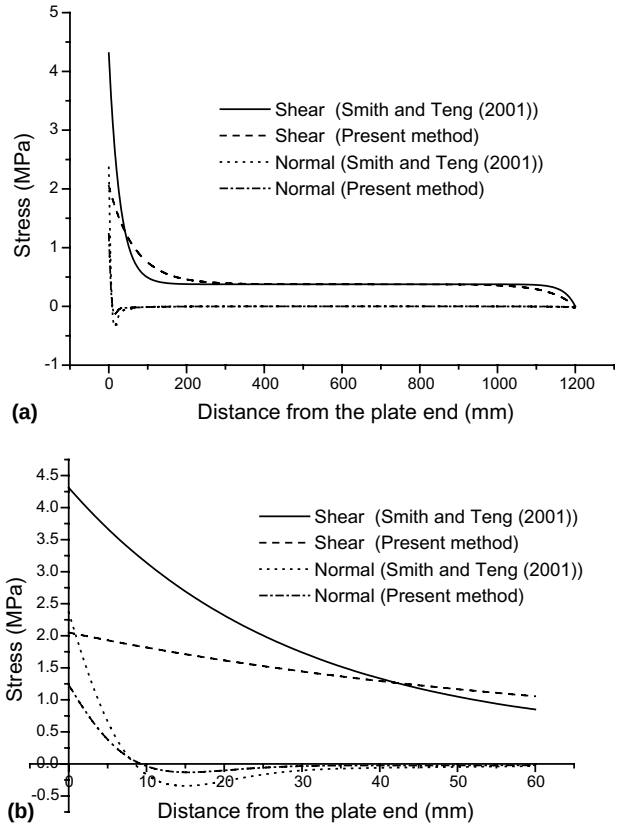

Fig. 6. Comparison of interfacial shear and normal stresses for an RC beam with a bonded CFRP soffit plate subjected to a mid-point load.

Table 3
Comparison of peak interfacial shear and normal stresses: UDL

Theory	RC beam with GFRP plate		RC beam with CFRP plate		RC beam with steel plate	
	τ (MPa)	σ_n (MPa)	τ (MPa)	σ_n (MPa)	τ (MPa)	σ_n (MPa)
Smith and Teng (2001)	2.392	1.640	3.834	2.100	4.443	2.247
Present	1.085	0.826	1.791	1.078	2.120	1.175

Table 4
Comparison of peak interfacial shear and normal stresses: mid-point load

Theory	RC beam with GFRP plate		RC beam with CFRP plate		RC beam with steel plate	
	τ (MPa)	σ_n (MPa)	τ (MPa)	σ_n (MPa)	τ (MPa)	σ_n (MPa)
Smith and Teng (2001)	2.677	1.837	4.310	2.364	5.003	2.533
Present	1.228	0.935	2.051	1.234	2.438	1.350

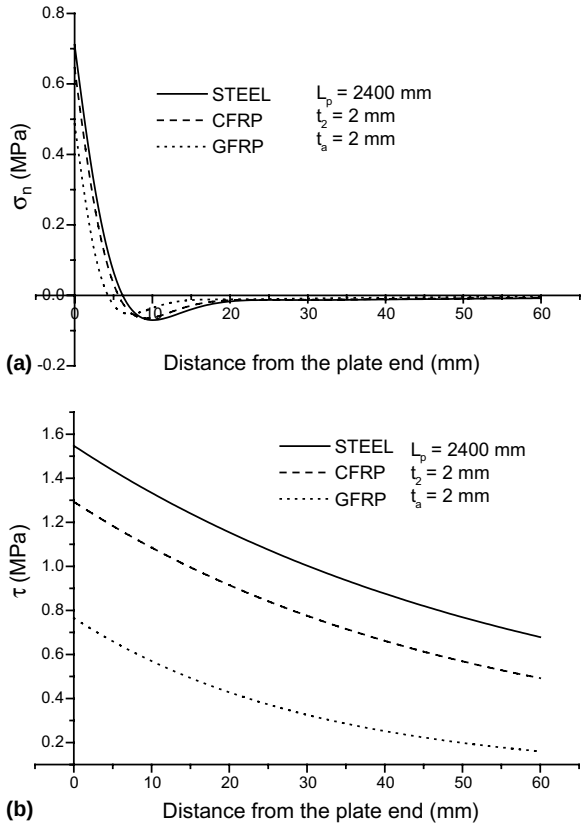

Fig. 7. Effect of plate material on interfacial stresses in strengthened beam: (a) normal stress; (b) shear stress.

from the results, the peak interfacial stresses assessed by the present theory are smaller compared to those given by Smith and Teng's solution (2001). This implies that adherend shear deformation is an important factor influencing the adhesive interfacial stresses distribution.

6. Interfacial stresses for different parameters

In this section, numerical results of the present solution are presented to study the effect of various parameters on the distributions of the interfacial stresses in an RC beam bonded with FRP or steel plate. These results are intended to demonstrate the main characteristics of interfacial stress distributions in these strengthened beams. The numerical results are presented in Figs. 7–10.

The example RC beam has a span of 3000 mm and the cross-sectional height $t_1 = 300$ mm. The material properties of the RC beam and the adhesive adopted in the parametric study are, respectively:

$$E_1^{(1)} = 30.0\ \text{GPa}, \quad v_{12}^{(1)} = 0.18 \quad \text{and} \quad E_a = 3.0\ \text{GPa}, \quad v_a = 0.35$$

The material of the strengthening plate was considered to one of the following three: glass fibre reinforced polymer (GFRP) composite, CFRP composite and steel.

All three layers have the equal width $b_2 = 200$ mm and the beam is subjected to a uniformly distributed load 50 kN/m.

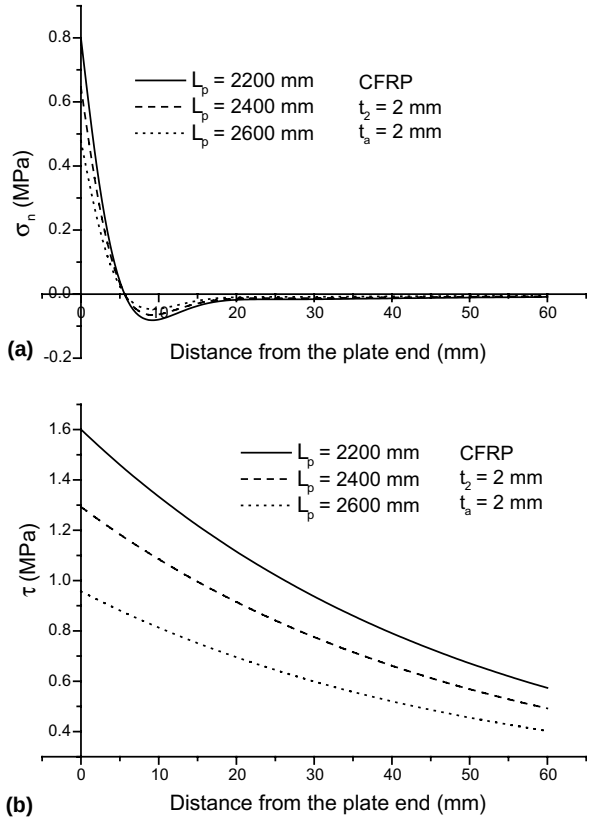

Fig. 8. Effect of plate length on interfacial stresses in CFRP-strengthened beam: (a) normal stress; (b) shear stress.

Fig. 7 gives interfacial normal and shear stresses for the RC beam bonded with a steel plate, CFRP plate and GFRP plate, respectively, which demonstrate the effect of plate material properties on interfacial stresses. The length of the plate is $L_p = 2400$ mm, and the thickness of the plate and the adhesive layer are both 2 mm. The results show that, as the plate material becomes softer (from steel to CFRP and then GFRP), the interfacial stresses become smaller, as expected. This is because, under the same load, the tensile force developed in the plate is smaller, which leads to reduced interfacial stresses. The position of the peak interfacial shear stress moves closer to the free edge as the plate becomes softer.

Fig. 8 shows the interfacial stresses for beams bonded with CFRP plates of different lengths ($L_p = 2200$, 2400 and 2600 mm, respectively). Again, the thicknesses of the plate and the adhesive layer are both *2* mm. It is seen that, as the plate terminates further away from the supports, the interfacial stresses increase significantly.

The effect of the thickness of the CFRP plate ($t_2 = 1$, 2 and 3 mm, respectively) on interfacial stresses is shown in Fig. 9, and the effect of the thickness of the adhesive layer ($t_a = 1$, 2 and 3 mm, respectively) is

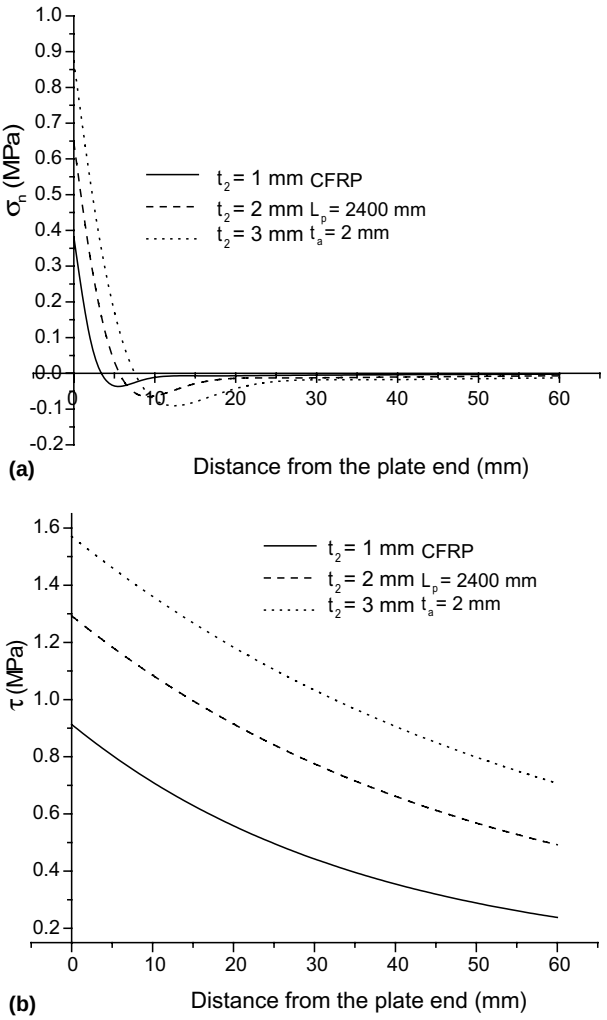

Fig. 9. Effect of plate thickness on interfacial stresses in CFRP-strengthened beam: (a) normal stress; (b) shear stress.

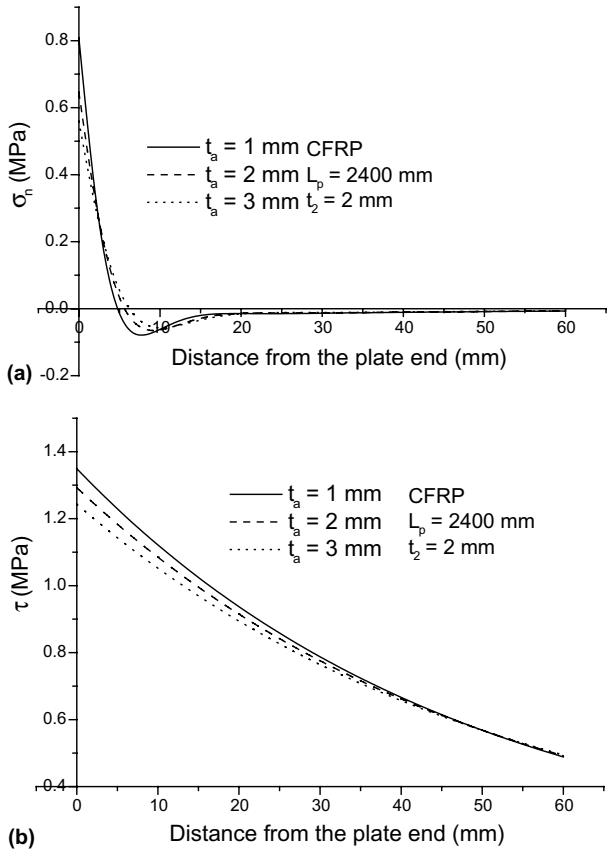

Fig. 10. Effect of adhesive layer thickness on interfacial stresses in CFRP-strengthened beam: (a) normal stress; (b) shear stress.

shown in Fig. 10. Both the normal and the shear stresses are increased as a result of an increase in the plate thickness. This effect is similar to that of an increase in the plate elastic modulus shown in Fig. 7. It can be seen from Fig. 10 that the thickness of adhesive layer affects only the normal and shear stress concentrations, hardly the stress levels. However, design of the properties and thickness of the adhesive is a difficult problem. An optimization design of the adhesive is expected.

7. Conclusion

The interfacial stresses in the FRP–RC hybrid beam were investigated by an improved theoretical method. The adherend shear deformations have been included in the theoretical analyses by assuming linear shear stress distributions through the thickness of the adherends. The classical solutions which neglect the adherend shear deformations over-estimate the non-uniformity of the adhesive stresses distributions and maximum interfacial stresses. The new solution is general in nature and may be applicable to all kinds of materials.

References

An, W., Saadatmanesh, H., Ehsani, M.R., 1991. RC beams strengthened with FRP plates: II. Analysis and parametric study. ASCE Journal of Structural Engineering 117 (11), 3434–3455.

Arduini, M., Nanni, A., 1997. Parametric study of beams with externally bonded FRP reinforcement. ACI Structural Journal 94 (5), 493–501.

Ascione, L., Feo, L., 2000. Modeling of composite/concrete interface of RC beams strengthened with composite laminates. Composites Engineering Part B 31, 535–540.

Bakis, C.E., Bank, L.C., Brown, V.L., Cosenza, E., Davalos, J.F., Lesko, J.J., 2002. Fiber-reinforced polymer composites for construction state-of-the-art review. ASCE Journal of Composites for Construction 6 (2), 73–87.

Baluch, M.H., Ziraba, Y.N., Azad, A.K., Sharif, A.M., Al-Sulaimani, G.J., Basunbul, I.A., 1995. Shear strength of plated RC beams. Magazine of Concrete Research 47 (173), 369–374.

Chajes, M.J., Thomson Jr., T.A., Januszka, T.F., Finch Jr., W.W., 1994. Flexural strengthening of concrete beams using externally bonded composite materials. Construction and Building Materials 8 (3), 191–201.

Chen, J.F., Teng, J.G., 2001. Anchorage strength models for FRP and steel plates bonded to concrete. ASCE Journal of Structural Engineering 127 (1), 784–791.

Chen, J.F., Teng, J.G., 2003. Shear capacity of FRP-strengthened RC beams: FRP debonding. Construction and Building Materials 17, 27–41.

Gao, B., Leung, C.K.Y., Kim, J.K., 2005. Prediction of concrete cover separation failure for RC beams strengthened with CFRP strips. Engineering Structures 27 (2), 177–189.

Jones, K.R., Swamy, R.N., Charif, A., 1988. Plate separation and anchorage of reinforced concrete beams strengthened by epoxy-bonded steel plates. The Structural Engineer 66 (5/1), 85–94.

Malek, M., Saadatmanesh, H., Ehsani, M.R., 1998. Prediction of failure load of R/C beams strengthened with FRP plate due to stress concentration at the plate end. ACI Structural Journal 95 (2), 142–152.

Oehlers, D.J., 1992. Reinforced concrete beams with plates glued to their soffits. ASCE Journal of Structural Engineering 118 (8), 2023–2038.

Quantrill, R.J., Hollaway, L.C., Thorne, A.M., 1996a. Experimental and analytical investigations of FRP-strengthened beam response: Part I. Magazine of Concrete Research 48 (177), 331–342.

Quantrill, R.J., Hollaway, L.C., Thorne, A.M., 1996b. Predictions of the maximum plate end stresses of FRP strengthened beams: Part II. Magazine of Concrete Research 48 (177), 343–351.

Rabinovich, O., Frostig, Y., 2000. Closed-form high order analysis of RC beams strengthened with FRP strips. ASCE Journal of Composites for Construction 4 (2), 65–74.

Raoof, M., El-Rimawi, J.A., Hassanen, M.A.H., 2000. Theoretical and experimental study on externally plated RC beams. Engineering Structures 22, 85–101.

Roberts, T.M., 1989. Approximate analysis of shear and normal stress concentrations in adhesive layer of plated RC beams. The Structural Engineer 67 (12), 229–233.

Roberts, T.M., Haji-Kazemi, H., 1989. A theoretical study of the behaviour of reinforced concrete beams strengthened by externally bonded steel plates. Proceedings of the Institution of Civil Engineers, Part 2 87, 39–55.

Saadatmanesh, H., Ehsani, M.R., 1991. RC beams strengthened with GFRP plates: I. Experimental study. ASCE Journal of Structural Engineering 117 (11), 3417–3433.

Saadatmanesh, H., Malek, A.M., 1998. Design guidelines for flexural strengthening of RC beams with FRP plates. ASCE Journal of Composites for Construction 2 (4), 158–164.

Sharif, A., Al-Sulaimani, G.J., Basunbul, I.A., Baluch, M.H., Ghaleb, B.N., 1994. Strengthening of initially loaded reinforced concrete beams using FRP plates. ACI Structural Journal 91 (2), 160–168.

Shen, H.S., Teng, J.G., Yang, J., 2001. Interfacial stresses in beams and slabs bonded with a thin plate. ASCE Journal of Engineering Mechanics 127 (4), 399–406.

Smith, S.T., Teng, J.G., 2001. Interfacial stresses in plated beams. Engineering Structures 23 (7), 857–871.

Smith, S.T., Teng, J.G., 2002a. FRP-strengthened RC beams. I: Review of debonding strength models. Engineering Structures 24 (4), 385–395.

Smith, S.T., Teng, J.G., 2002b. FRP-strengthened RC beams. II: Assessment of debonding strength models. Engineering Structures 24 (4), 397–417.

Spadea, G., Bencardino, F., Swamy, R.N., 1998. Structural behavior of composite RC beams with externally bonded CFRP. ASCE Journal of Composites for Construction 2 (3), 132–137.

Taljsten, B., 1997. Strengthening of beams by plate bonding. ASCE Journal of Materials in Civil Engineering 9 (4), 206–212.

Triantafillou, T.C., Antonopoulos, C.P., 2000. Design of concrete flexural members strengthened in shear with FRP. ASCE Journal of Composites for Construction 4 (4), 198–205.

Tsai, M.Y., Oplinger, D.W., Morton, J., 1998. Improved theoretical solutions for adhesive lap joints. International Journal of Solids and Structures 35 (12), 1163–1185.

Wu, Z., Matsuzaki, T., Tanabe, K., 1997. Interface crack propagation in FRP-strengthened concrete structures. Non-metallic (FRP) Reinforcement for Concrete Structures, vol. 1, Japan Concrete Institute, pp. 319–326.

Wu, Z., Yuan, H., Niu, H., 2002. Stress transfer and fracture propagation in different kinds of adhesive joints. ASCE Journal of Engineering Mechanics 128 (5), 562–573.

Yang, J., Chen, J.F., Teng, J.G., 2002. Interfacial stresses in plated RC beams under arbitrary symmetric load: A higher-order closed form solution. In: Proceedings of the First International Conference on the use of Advanced Composites in Construction, Southampton University, UK, pp. 153–163.

Yuan, F., Teng, J.G., Seracino, R., Wu, Z.S., Yao, J., 2004. Full-range behaviour of FRP-to-concrete bonded joints. Engineering Structures 26, 553–565.